Characterization of the non-crystalline phase of oriented poly(ethylene terephthalate) by chain-intrinsic fluorescence

B. Clauss* and D. R. Salem†
TRI/Princeton, PO Box 625, Princeton, NJ 08542, USA
(Received 13 August 1991; accepted 25 September 1991)

We have investigated the suitability of the chain-intrinsic fluorescent properties of poly(ethylene terephthalate) for characterizing 'amorphous orientation' in semicrystalline films and fibres of this polymer. By developing an apparatus which permits the polarized fluorescence to be measured in the optical axis, we have eliminated possible sources of measurement error. Our results provide further evidence that the increase in fluorescence intensity at high draw ratios arises from light scattering between crystallites and not from an increase in the population of fluorescent dimers. This cause of intensity increase would have no influence on the orientation function, and one can correct for any significant depolarization due to scattered light. For hot-drawn film, the amorphous orientation data obtained from intrinsic fluorescence provide a consistent explanation of the influence of strain rate on the induction and development of crystallinity. For fibres, our intrinsic fluorescence data confirm that high speed spinning results in substantially lower amorphous orientation than spin-drawing, and that amorphous orientation goes through a maximum as a function of spinning speed. These fluorescence results are in very good qualitative agreement with data we obtained from a birefringence/X-ray method; quantitative differences seem to arise from the choice of values for intrinsic birefringence (Δ_c^o and Δ_a^o) required in the latter method. Determination of Δ_c^o and Δ_a^o using amorphous orientation data from the fluorescence method provides support for the argument that these values are not truly intrinsic, but are dependent on the structural state of the crystalline and amorphous regions.

(Keywords: poly(ethylene terephthalate); non-crystalline phase; chain-intrinsic fluorescence; amorphous orientation; film; fibres)

INTRODUCTION

Although it is well recognized that the physical properties of semicrystalline polymers can be critically dependent on the state of order in the non-crystalline regions, quantitative assessment of this dependence remains elusive due to experimental difficulties in measuring 'amorphous orientation' reliably. Techniques based on measurement of the optical birefringence and the sonic modulus of the polymer are frequently used, but these are indirect methods requiring detailed characterization of the crystalline phase and involving some controversial assumptions.

The first systematic attempts to explore the application of polarized fluorescence to the measurement of orientation in polymers are due to the pioneering work of Nishijima *et al.*[1–8]. The basic theory of fluorescence polarization has been developed by Desper and Kimura[9] and has been extended for the uniaxial case by Nobbs *et al.*[10]. Other contributions to the theoretical background have been given by Stein[11] and by White and Spruiell[12] for biaxial orientation. Most of the work has been done with fluorescent probe molecules incorporated in the polymer either before melting and extrusion or afterwards in a dyeing process. It has been assumed that the long rod-like probes are aligned with the polymer chain and therefore reflect the orientation of these chains. Since the probes cannot be incorporated into crystallites, this method can be used to determine orientation in the non-crystalline regions of semicrystalline polymers. It should be pointed out, however, that the probes are not necessarily perfectly aligned with the polymer chain, and the degree of alignment may change during deformation. Moreover, some results[13] indicate that the fluorescent probes align preferentially with chain segments in the *trans* conformation so that this method does not measure the average amorphous orientation.

Recently it has been shown that an associated ground state dimer of poly(ethylene terephthalate) (PET), consisting of two terephthalic moieties and forming exclusively within amorphous regions, can be used as a *chain-intrinsic* fluorescent label reflecting amorphous orientation[14–18]. By using the intrinsic fluorescence of the PET chain, probe alignment problems are avoided, and this technique would be expected to yield the *average* orientation of chains in the amorphous regions. Moreover, it has been established that the fluorescent site does not change its properties during extension of the polymer[16]. There is evidence, however, that fluorescence intensity increases somewhat at high extensions. Although this increase does not influence the results, since the

*Present address: DITF, Institut für Textilchemie, Körschtalstr. 26, 7306 Denkendorf, Germany
†To whom correspondence should be addressed

0032-3861/92/153193-10

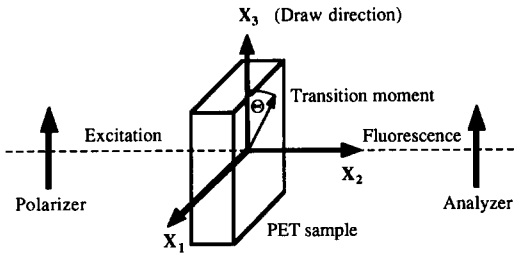

Figure 1 Schematic diagram of fluorescence experiment

orientation distributions are obtained from intensity ratios and normalized by the total fluorescence intensity, its origins are of interest and will be discussed in the present work. Our main purposes are to report a novel experimental set-up which significantly enhances the accuracy and convenience of the intrinsic fluorescence technique, and to present some preliminary orientation data for hot-drawn film and for high speed spun and spun-drawn fibres, which help to assess the suitability of the technique.

THEORY

Fluorescence emission from PET in the range 360–420 nm has been attributed to an associated ground state dimer occurring in uncrystallized regions[15–18]. To emit strongly in this range, the dimers must be excited[15,16] at a wavelength around 340 nm; the emission spectrum then has a maximum around 390 nm. Using polarized incident light and measuring the polarized components of the fluorescent light, one can calculate the orientation of the fluorescent elements.

The absorption probability for the incident light is proportional to the square of the projection of the absorption moment of a molecule into the direction of the electrical field, i.e. it is proportional to the square of the cosine of the angle between the absorption moment and the electric vector of the incident light. The intensity of the detected fluorescent light is proportional to the square of the cosine of the angle between the emission moment and the direction of the analysing polarizer. *Figure 1* diagrams the fluorescence experiment, defining the principal coordinate axes. In polarized fluorescence analysis, certain requirements must be met or corrections made, as follows.

1. No rotational motion of the fluorescent element relative to the chain axis during the fluorescence lifetime ($\sim 10^{-8}$ s) is permissible. In the case of chain-intrinsic fluorescence this requirement is clearly met. For incorporated fluorescent probes, the work of Nobbs *et al.* indicates that no rotational motion occurs at temperatures below the glass transition[10].
2. The transition moments in both absorption and emission must coincide with the molecular axis of the fluorescent element and with the molecular axis of the polymer chain. Two possibilities should be considered. First, the fluorescent element itself may not be completely aligned with the polymer chain. Second, the absorption and emission axes may not coincide with the molecular axis within the fluorescent element. In the case of incorporated probe molecules, misalignment with the polymer chain is likely, but since it is very difficult to quantify the degree of misalignment, this complication is usually neglected. Obviously this problem can be avoided by using chain-intrinsic fluorescence, which can be seen as one of the main advantages of this technique. Concerning the second possibility: deviation of the absorption and emission axes from the molecular axis and an optical anisotropy of the absorption and emission tensors can be present with both extrinsic and chain-intrinsic fluorescent elements. Assuming the coincidence of absorption and emission moments and using some additional assumptions concerning the tensor symmetries[19], a correction can be devised for incomplete emission anisotropy. Incomplete emission anisotropy means that the fluorescent chain segment emits light not only with one distinct polarization direction but also polarized in other directions. The degree of emission anisotropy can be determined by measuring certain intensity ratios in an unoriented specimen[20], because these specimens have a known (random) distribution of fluorescent sites. Maximum emission anisotropy, i.e. completely polarized emission in one direction, would result in $r_0 = 0.4$, and completely isotropic emission would result in $r_0 = 0$. For PET, r_0 appears to be in the region 0.30–0.35, and the correction procedure devised by Hennecke and Fuhrmann[20] is given later [equations (9)–(13)]. In making this correction it is assumed that the emission anisotropy does not depend on the molecular orientation, and therefore the value determined for unoriented specimens can be used for correcting specimens of any orientation.
3. The state of polarization of the excitation and fluorescence lights must not be changed by birefringence or scattering. A correction for birefringence is important if intensities are measured at different angles. The highest influence would be with the polarizers at 45° to the draw direction. Birefringence can be ignored, however, if the intensities are measured only at 0° and 90° to the draw direction, i.e. with the polarizers in 33-, 31-, 13- or 11-positions[10,21,22]. If the light is depolarized within the specimen due to scattering by crystallites or other entities, the results should also be corrected for this effect. A proposed correction procedure is given by Hennecke[19] and by Pinaud *et al.*[21].

The arguments involved in obtaining orientation functions from polarized fluorescence are summarized as follows.

The fluorescence intensities I_{ij} for uniaxial stretched specimens (along X_3) measured with the polarizer along X_i and the analyser along X_j are given by:

$$I_{33} = K\langle\cos^4\Theta\rangle \tag{1}$$

$$I_{31} = I_{13} = (K/2)\langle\cos^2\Theta\sin^2\Theta\rangle = (K/2)\langle\cos^2\Theta - \cos^4\Theta\rangle \tag{2}$$

$$I_{11} = (3K/8)\langle\sin^4\Theta\rangle \tag{3}$$

where the angled brackets denote an ensemble average over all fluorescent elements. As shown by Desper and Kimura[9], the result of the normalization condition

$$\sum_{i=1}^{3}\sum_{j=1}^{3} I_{ij} = 1 \tag{4}$$

which is

$$I_{33} + 4I_{31} + (8/3)I_{11} = 1 \tag{5}$$

for uniaxial symmetry, can be used for normalizing the intensities by defining:

$$I_{33} + 4I_{31} + (8/3)I_{11} = K \quad (6)$$

The second and fourth moment of the orientation distribution can then be calculated from equations (1)–(3):

$$\langle \cos^2 \Theta \rangle = \frac{I_{33} + 2I_{31}}{I_{33} + 4I_{31} + (8/3)I_{11}} \quad (7)$$

$$\langle \cos^4 \Theta \rangle = \frac{I_{33}}{I_{33} + 4I_{31} + (8/3)I_{11}} \quad (8)$$

By including Hennecke and Fuhrmann's correction for emission anisotropy[20], equations (7) and (8) become:

$$\langle \cos^2 \Theta \rangle = 1/2 + (1/2)\langle \cos^4 \Theta \rangle - \frac{16(1-p)I_{11}/K + 4pI_{33}/K - 4p(1-p)}{(2-3p)^2(3-p)} \quad (9)$$

$$\langle \cos^4 \Theta \rangle = \frac{16pI_{11}/K + (12-10p)I_{33}/K - p(6-7p+3p^2)}{(2-3p)^2(3-p)} \quad (10)$$

with

$$K = \frac{(3-2p)I_{33} + 8I_{11} + 4(3-p)I_{31}}{3-2p+p^2} \quad (11)$$

In these formulae the optical anisotropy p is used instead of r_o. These quantities are related by:

$$p = 2/3 - (1/3)(10r_o)^{1/2} \quad (12)$$

The emission anisotropy, for unoriented isotropic specimens, is calculated from:

$$r_o = \frac{I_{33} - I_{31}}{I_{33} + 2I_{31}} \quad (13)$$

The second and fourth moments of the orientation function can then be calculated from:

$$\langle P_2(\cos \Theta) \rangle_{a/fl} = (1/2)\langle 3\cos^2 \Theta - 1 \rangle \quad (14)$$

$$\langle P_4(\cos \Theta) \rangle_{a/fl} = (1/8)\langle 3 - 30\cos^2 \Theta + 35\cos^4 \Theta \rangle \quad (15)$$

Correction for depolarization due to scattering of light from opaque specimens, if significant, involves the measurement of scattering factors for the excitation and fluorescence wavelengths[19,21].

EXPERIMENTAL

Apparatus

For fluorescence measurements in solution it is usual to measure the fluorescence intensity at 90° to the excitation direction so that the very intense excitation light does not disturb the measurement. This is not possible if one uses thin specimens, like fibres and films, in which case it is necessary to suppress the excitation light as completely as possible. The easiest way to achieve this suppression is to tilt the detector slightly (5°) relative to the optical axis and to cut off the excitation light with a beam stop, which covers one side of the detector area. However, we found problems with this arrangement.

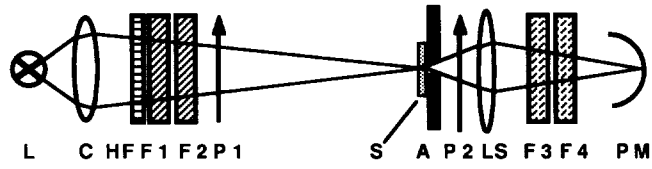

Figure 2 Experimental set-up for measurement of polarized intrinsic fluorescence: L, mercury arc lamp; C, condenser; HF, heat filter; F1, F2, interference filters (334 nm); P1, P2 near u.v. polarizers; S, PET specimen; A, aperture; LS, lens system; F3, F4, interference filters (390 nm); PM, photomultiplier

Photomultipliers are known to have different sensitivities for light at different polarization directions, so that a correction is necessary if the analyser is rotated. To avoid this correction, the specimen can be rotated while keeping the analyser in a fixed position. The fluorescence light distribution behind the specimen is not uniform, however, especially if the polymer is oriented; i.e. the emission of an oriented specimen is not spherical but has a higher intensity perpendicular to the draw direction than parallel to it. For this reason the asymmetrical arrangement – tilted detector with a beam stop at one side – does not permit measurement by rotating the specimen.

A simple solution for this problem was the use of a round beam stop in the centre of the detector, which had the proper diameter to block all the excitation light. This also had the advantage that more fluorescence light reached the detector (in the case of the tilted detector not only the excitation light is blocked, but also a significant amount of fluorescence light). With this symmetrical arrangement the specimen can be rotated without problems arising from non-uniform fluorescence light distribution. However, another problem remained: if the specimens are not completely clear, scattering causes a broad distribution of excitation light to reach the detector. Consequently, the boundary line between the excitation light and the fluorescence light becomes indistinct, and it is no longer possible to be certain that the beam stop cuts all excitation light.

By abandoning the beam stop arrangement altogether, it was possible to solve both the excitation light and the boundary-line problems. A much more effective filter arrangement was installed for the excitation and fluorescent wavelengths, involving two filters in series, and a lens system with a very short focal length was placed close to the aperture. As a result, the fluorescence intensity becomes significantly higher than the intensity of the excitation light, even when measuring in the optical axis without a beam stop. The photomultiplier can then be adjusted to zero photocurrent without a specimen, and any signal obtained with a specimen in place can only arise from the fluorescence light. In this case no corrections for excitation light or detector sensitivity are necessary.

The final experimental arrangement is shown in *Figure 2*. The analyser P2 remains in a fixed position during the measurements, while the polarizer P1 and the specimen are rotated. Intensities are measured at 0° and 90° to the draw direction, so that no correction for birefringence is required (see Theory).

Materials

Amorphous, undrawn PET film ($\bar{M}_n = 19000$) was supplied by Rhône Poulenc. It has been described in

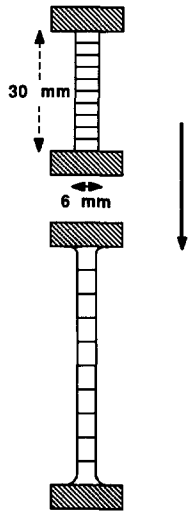

Figure 3 Specimen geometry of PET film, before and after drawing

Table 1 Volume fraction crystallinity of high-speed spun and spun-drawn fibres

Winding speed (m min^{-1})	Crystallinity
3200	0.05
4100	0.12
4500	0.19
5500	0.25
6000	0.25
7000	0.24
Draw ratio	
3.8	0.26
4.2	0.27
4.6	0.28
5.0	0.26
4.2 (Du Pont)	0.33

detail elsewhere[23]. The amorphous film was uniaxially deformed to various draw ratios on an Instron tensile tester. A draw temperature of 90°C and strain rates of 0.01 and 0.56 s^{-1} were used. The specimen geometry of the undrawn film was such that the deformation mode was essentially simple extension (*Figure 3*). Thus, the molecules and crystallites in the drawn film are uniaxially oriented; as in drawn fibres, they are randomly oriented about their own axes. This differs from the constant-width (pure shear) deformation of our previous studies[23,24], which results in both axial and planar orientation. (With our present intrinsic-fluorescence set-up, we cannot obtain a complete description of amorphous orientation in constant-width specimens – only the axial, in-plane orientation.)

The PET fibres used were from four Du Pont yarns, spun at speeds in the range 3200–5500 m min^{-1}, two Toray yarns spun at 6000 and 7000 m min^{-1}, a conventionally spun and drawn Du Pont yarn (Dacron® 55) with a draw ratio of 4.2, and four Enka yarns with draw ratios of 3.8, 4.2, 4.6 and 5.0. The Enka yarns were manufactured by a two-stage drawing process, with the first draw at 120°C and the second at 160°C. The crystallinities of these fibres, estimated from equation (17), are given in *Table 1*. The number average molecular weights are all in the range 18 000–23 000.

Procedures

Polarized intrinsic-fluorescence method. For orientation measurements of film, a single segment of the drawn sample was used. For fibres, four to five lengths of yarn were cut from the package, and then spread out and mounted on a cardboard frame. For adequate fluorescence intensity, it was necessary to have about 100 single filaments in the beam. Care was taken to maximize parallel alignment and to minimize the gap between filaments. After placing the specimen over the aperture (*Figure 2*), the I_{33}, I_{31}, I_{13} and I_{11} intensities were measured by rotating the polarizer and the specimen, keeping the analyser fixed.

The fibre and film specimens can be somewhat opaque due to light scattering from crystallites and/or TiO_2 particles. TiO_2 was present in the fibres but not the film. Since light scattering could cause significant depolarization, the correction procedure formulated by Pinaud *et al.*[21] was applied. The results of this procedure showed that the level of scattering from our specimens causes negligible depolarization. From this it can be deduced that any light scattering between filaments, due to their cylindrical geometry, does not produce significant depolarization either.

As discussed earlier (see Theory), it is necessary to measure the emission anisotropy r_0 of an unoriented specimen. For the unoriented film, a value of $r_0 = 0.3$ was obtained. Since we did not have an unoriented specimen from the series of fibres studied, we used the value obtained from the film. For PET, r_0 appears to range between 0.3 and 0.35, but using $r_0 = 0.35$ would have reduced our calculated values of the orientation function $\langle P_2(\cos\Theta)\rangle_{a/fl}$ by only 2–4%.

We found low experimental scatter in the orientation function for drawn PET film, and each datum point in the film study represents a single specimen. For fibres, however, it was necessary to take readings from five to ten specimens in order to keep the coefficient of variation to ~5%. The lower reproducibility of data obtained from fibres probably arises from the difficulties involved in mounting and aligning single filaments with precision.

Birefringence/X-ray method. Amorphous orientation from birefringence, $\langle P_2(\cos\Theta)\rangle_{a/bir}$, was calculated from:

$$\Delta = \Delta_c^\circ \chi \langle P_2(\cos\Theta)\rangle_c + \Delta_a^\circ (1-\chi)\langle P_2(\cos\Theta)\rangle_{a/bir} \tag{16}$$

where Δ is the total optical birefringence of the specimen[25]. The intrinsic birefringences of the crystalline and amorphous phases, Δ_c° and Δ_a°, were taken as 0.22 and 0.275, respectively[26]. Birefringence was measured by interference microscopy. The crystalline orientation factor, $\langle P_2(\cos\Theta)\rangle_c$, was determined from wide-angle X-ray scattering (WAXS), using the off-meridional $\bar{1}05$ reflection. The volume fraction crystallinity χ was calculated from density measurements, as detailed in the next section.

Crystallinity determinations. Volume fraction crystallinity was calculated from:

$$\chi = \frac{(\rho - \rho_a)}{(\rho_c - \rho_a)} \tag{17}$$

The bulk density of the polymer ρ was measured using

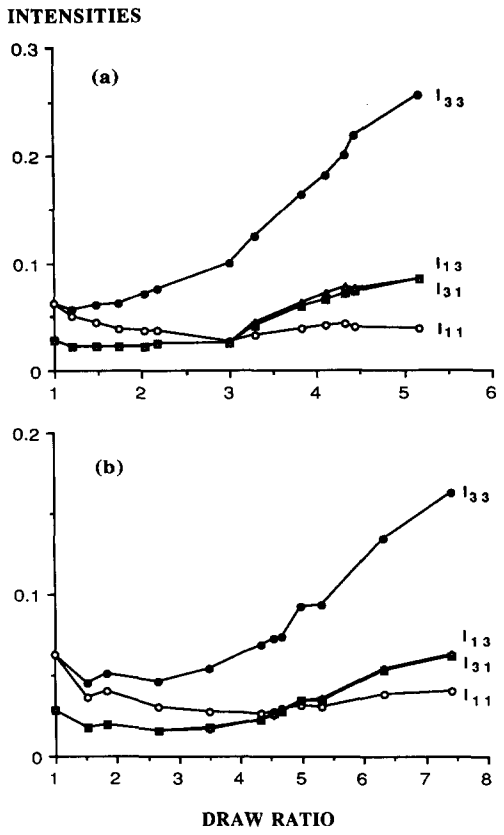

Figure 4 Measured fluorescence intensities for different polarizer and analyser positions. Strain rates are (a) 0.56 s^{-1} and (b) 0.01 s^{-1}

a density gradient column. In the case of the fibre specimens, WAXS revealed some significant process-dependent variations in lattice spacings. Therefore, the crystalline density ρ_c was calculated for each specimen from the 2Θ position of the equatorial 010, $\bar{1}10$ and 100 reflections and from the off-meridional $\bar{1}05$ reflection. In this analysis, a four-line profile-fitting procedure similar to that of Heuvel and Huisman[27–29] was used to resolve the equatorial crystalline reflections and the amorphous scattering, and it was assumed that the crystallographic angles α, β and γ do not change significantly[29,30]. Where necessary, corrections were made for the influence of small crystal size on the 2Θ positions of the reflections, as discussed elsewhere[31,32]. The amorphous density ρ_a was assumed to be 1335 kg m^{-3} in the absence of additive, and was adjusted according to the weight fraction of TiO_2 present.

In the case of the film specimens, no significant variations in lattice spacings were evident for the range of drawing conditions used, and ρ_c was taken as 1457 kg m^{-3}. Since the film did not contain TiO_2 or other additives, ρ_a was taken as the density of the undrawn film (1339 kg m^{-3})[23].

RESULTS AND DISCUSSION

Hot-drawn film

Fluorescence measurements were made on two series of PET film samples, which had been drawn at strain rates of 0.56 and 0.01 s^{-1}. Both series were drawn at a temperature of 90°C and were air-quenched after drawing. There was no further treatment of the specimens before taking the measurements.

Figure 4 shows the dependence of the measured intensities on draw ratio, and *Figure 5* the normalized total fluorescence intensity, K/d, where d is the specimen thickness. There is clearly a large change in slope at draw ratios of ~3.0 and ~4.4 for strain rates of 0.56 and 0.01 s^{-1}, respectively, and this phenomenon coincides with the onset of perceptible sample opaqueness. A possible interpretation of the increase in fluorescence intensity would be that it arises from an increase in the number of fluorescent dimers at higher orientations. On the other hand, Hennecke *et al.*[15,16] suggest that it arises from scattering between crystallites, causing an increase in the 'excited volume'; in other words, there is an increase in the length of the light path through the sample due to scattering, which is equivalent to an increase in sample thickness. These two possibilities will be discussed further, after presenting the orientation data.

The second moment of the orientation function is plotted *versus* draw ratio in *Figure 6a*. We have not drawn curves through the data because in a subsequent paper we will examine the low-strain region in considerable detail, using a larger number of data points. For the present, we wish to draw attention to various features of the orientation data which seem to be consistent with our crystallinity results.

We previously reported that the development of crystallinity during hot-drawing of PET film in *pure shear* is characterized by two crystallization regimes[23]: in regime 1, crystallinity develops more rapidly, and at much lower stress levels than in regime 2. *Figures 6b* and *7*, and other data[30], reveal that similar behaviour occurs during hot-drawing in *simple extension*. Relationships between amorphous orientation development and crystallinity development are evident from *Figure 6*. Amorphous orientation develops more slowly at lower strain rate, due to molecular relaxation during drawing, and there is a critical orientation for the onset of crystallization. Decreasing strain rate, therefore, shifts the onset of crystallization to higher draw ratios and reduces the rate at which crystallinity increases with draw ratio. These observations support the data of Le Bourvellec *et al.*[33], who determined amorphous orientation by incorporating a fluorescent probe molecule during polycondensation. It is noteworthy, however, that the chain-intrinsic fluorescence analysis gives a critical orientation for crystallization of ~0.17, whereas at the draw temperature of 90°C, Le Bourvellec

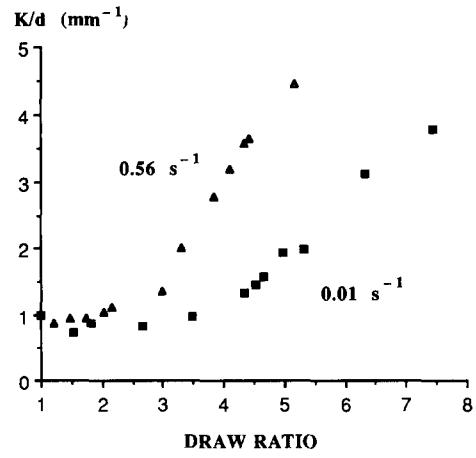

Figure 5 Normalized total fluorescence intensity *versus* draw ratio at two strain rates

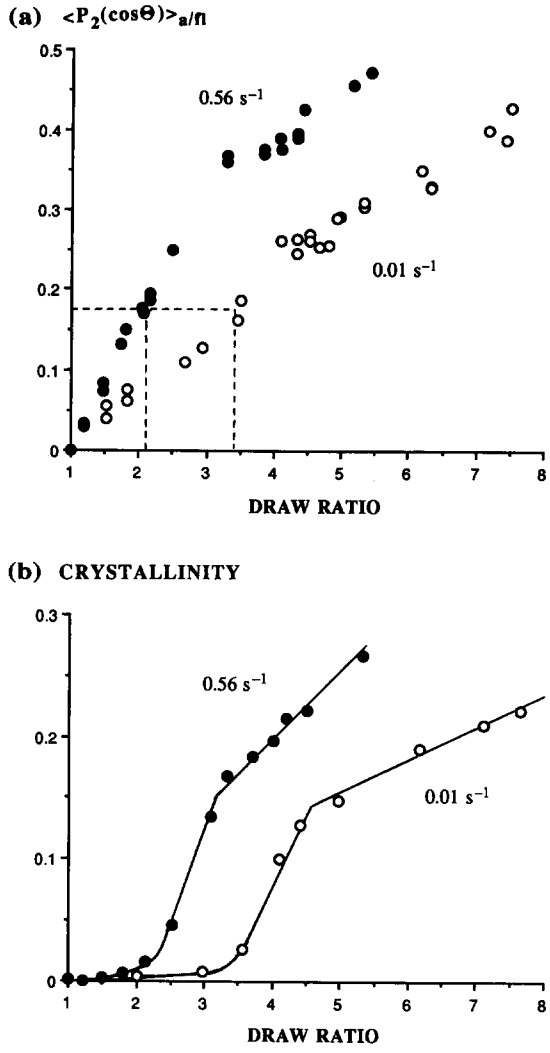

Figure 6 Development of (a) amorphous orientation from intrinsic fluorescence and (b) crystallinity, during drawing of PET film at 90°C, showing the influence of strain rate. The critical orientation for onset of crystallization is indicated

et al. found a value of 0.2. The difference is small, but may reflect a tendency for the incorporated fluorescent probe to align preferentially with chains in the *trans* conformation[13], as mentioned earlier.

Another interesting feature of *Figure 6* is the abrupt decrease in the rate of orientation development at a draw ratio which coincides with the onset of the second crystallization regime. It is perhaps curious that the generation of non-crystalline orientation is so slow in regime 2, when the stresses in this regime are particularly high. One could speculate, however, that after the formation of an 'effective' crystallite network, to which we attribute the steep rise in stress[23], the restricted mobility of the tie-chains would reduce their ability to extend and orient. For example, as soon as one of the tie-chains in an intercrystalline region becomes fully extended and able to transfer stress, all other tie-chains in that region would be unable to extend (*Figure 8*). There may also be considerable entanglement slippage in the high stress region, involving translational slippage between 'tie-segment blocks'[34] (*Figure 8*). Deformation mechanisms of this type would permit high macroscopic extension without requiring comparable extension and orientation of individual chains.

The orientation data can help to interpret the increase in fluorescence intensity at high draw ratios seen in *Figure 5*. It is important to consider the notion that the intensity increase arises from an orientation-induced increase in the number of fluorescent dimers. This would imply that dimers are preferentially formed by more highly oriented chain segments and that chains in the *trans* conformation may have a disproportionate influence on the orientation function. Our data, when plotted as in *Figure 9*, seem to show an upward trend in fluorescence intensity with increasing orientation. However this cannot be interpreted as true functional dependence of fluorescence intensity on the level of orientation achieved, since the 'scatter' in the data points in the high orientation range is much greater than can be attributed to experimental error. For example, when $\langle P_2(\cos\Theta)\rangle_{a/fl}$ is ~ 0.35, K/d is 1.7 at the high strain rate and 3.5 at the low strain rate – a difference which is at least 20 times larger than the experimental error. Clearly, strain rate should have no effect if there were a functional dependence of K/d on $\langle P(\cos\Theta)\rangle_{a/fl}$. *Figure 9*, therefore, provides strong evidence that increasing orientation does not result in an increase in the population of fluorescent dimers.

On the other hand, it seems significant that the abrupt increase in fluorescence intensity occurs at the onset of the second crystallization regime and that, in this regime, K/d is directly dependent on the level of crystallinity (*Figure 10*). This result, together with the onset of measurable specimen opaqueness at the onset of regime 2, supports other evidence[15,16] that the increased fluorescence intensity arises from an increase in excited volume, due to scattering of light between crystallites. It

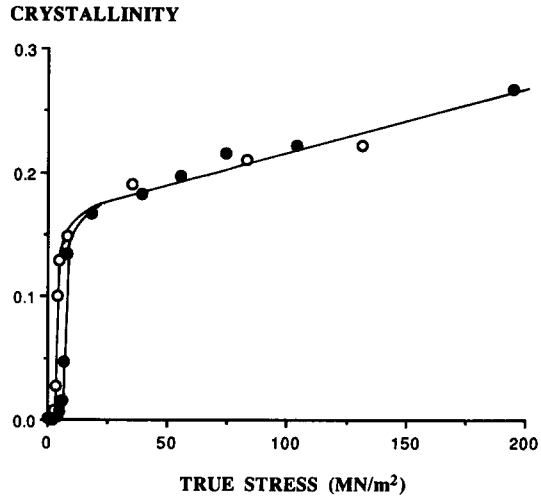

Figure 7 Crystallinity *versus* true stress for drawing of PET film at 90°C. Strain rates are 0.56 s^{-1} (●) and 0.01 s^{-1} (○)

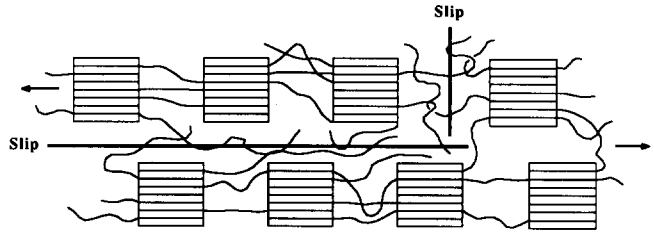

Figure 8 Speculative mechanism for extension of PET film in the high stress regime, involving translational slippage between 'tie-segment blocks'[34]

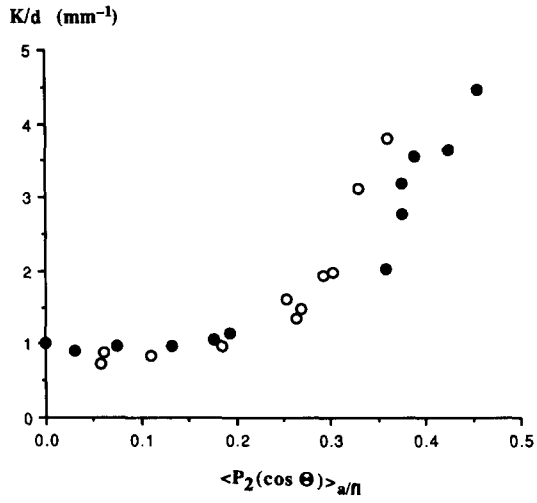

Figure 9 Normalized total fluorescence intensity *versus* $\langle P_2(\cos\Theta)\rangle_{a/fl}$, for strain rates of 0.56 s^{-1} (●) and 0.01 s^{-1} (○) and a draw temperature of 90°C

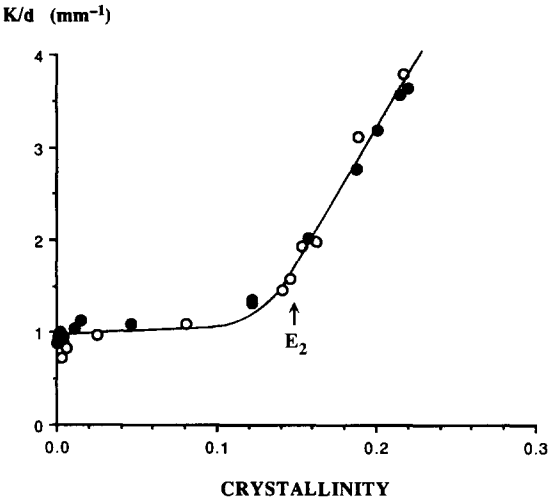

Figure 10 Normalized total fluorescence intensity *versus* crystallinity developed during drawing at 90°C. Strain rates are 0.56 s^{-1} (●) and 0.01 s^{-1} (○). The onset of crystallization regime 2 (E_2) is indicated

also emphasizes the distinctiveness of the two crystallization regimes: in regime 1, the level of crystalline order is insufficient to produce light scattering; in regime 2, the crystallites that form the network have sufficient size, orientation, number and regularity of spacing to act as effective light-scattering centres.

The crystallinity dependence of K/d also provides a reason for the larger intensity increase in our specimens, compared with those of Hennecke *et al.*[16]. Whereas our specimens were non-crystalline before drawing, the undrawn specimens of Hennecke *et al.* had a volume fraction crystallinity of 0.27, increasing by ~30% at the highest draw ratio. If light scattering from these specimens was already significant in the undrawn state, due to the high level of crystallinity, then this, together with the smaller increase in crystallinity during drawing, would explain their smaller fractional increase in fluorescence intensity at high draw ratios.

Despite strong evidence that fluorescence emission in the region 360–420 nm arises from non-crystalline regions[15–17,35], a tempting interpretation of the crystallinity–intensity relationship might be that crystallites somehow become fluorescence emitters at the onset of regime 2. If this were so, *Figure 10* would indicate that at the highest draw ratios there are roughly four times the number of fluorescent sites in the crystalline fraction than in the non-crystalline fraction, and the crystalline orientation would therefore dominate the result. Since we know from X-ray analysis that the crystallites in regime 2 are almost fully oriented[30], and if we suppose for the sake of argument that amorphous orientation never exceeds 0.2, we can calculate that the highest draw ratios would produce overall orientation values of ~0.8. However, our measured orientation values never exceed 0.45. We can therefore discount the idea that the increased fluorescence intensity is due to emission from crystalline regions.

High-speed spun and spun-drawn fibres

Data from the intrinsic fluorescence method confirm that amorphous orientation in high-speed spun fibres (*Figure 11*) is substantially lower than in spun-drawn fibres (*Figure 12*), and that amorphous orientation reaches a maximum at ~6000 m min^{-1} (references 36 and 37). It is also evident that the fluorescence results are in very good qualitative agreement with the results obtained from the birefringence/X-ray method. Considering that these two methods of determining amorphous orientation involve entirely different measurements and dissimilar assumptions, the level of agreement between them is encouraging. It is important to notice, however, that for the high-speed spun fibres, the absolute values of orientation obtained from intrinsic fluorescence are higher than those from birefringence, whereas for the spun-drawn fibres there is close quantitative agreement. These results suggest that incorrect values of the intrinsic birefringences, Δ_c° and Δ_a°, were used to calculate $\langle P_2(\cos\Theta)\rangle_{a/bir}$ for the high-speed spun fibres [equation (16)], and they provide evidence for the argument that Δ_c° and Δ_a° are not constant, as generally assumed, but depend on the microstructural state of the PET material.

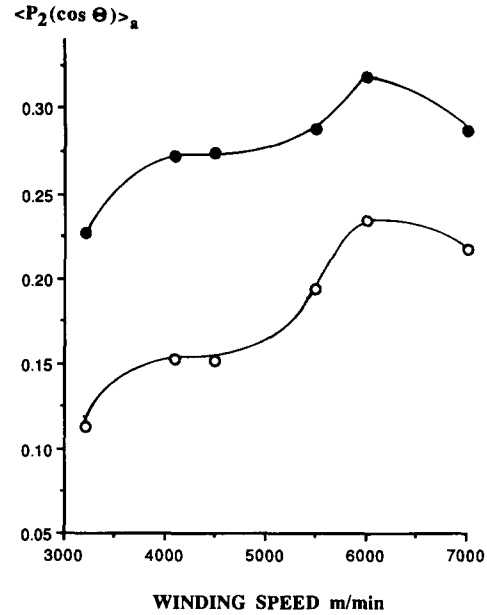

Figure 11 Influence of winding speed on amorphous orientation in high-speed spun fibres, as measured by intrinsic fluorescence (●) and birefringence/X-ray (○)

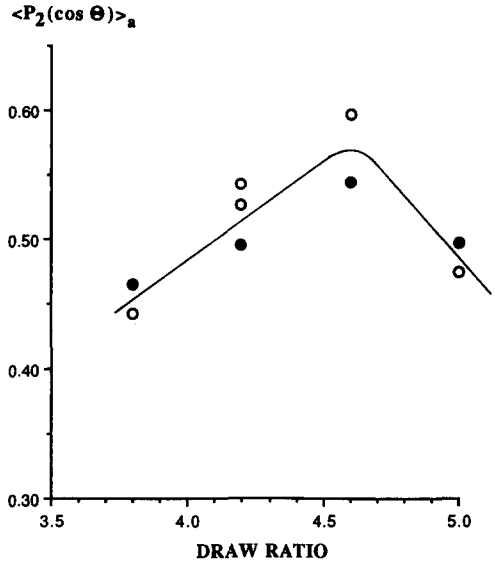

Figure 12 Influence of draw ratio on amorphous orientation, as measured by intrinsic fluorescence (●) and birefringence/X-ray (○). Most of the fibres were produced by a two-stage, high temperature drawing process (see Materials)

In a semicrystalline polymer, Δ_c^o and Δ_a^o can be defined as the birefringence of a perfectly oriented chain in, respectively, the crystalline and the amorphous phases. Ideally, therefore, they would have constant values for a given polymer. Stein has pointed out, however, that the polarizability of a chain is influenced by the induced dipolar field of neighbouring chains, and that the induced field depends on the orientation and configuration of those chains[38]. Thus, the birefringence of a fully oriented chain would be influenced by the orientation and packing density of neighbouring chains. This not only results in values of Δ_c^o and Δ_a^o which differ from each other, but implies that Δ_a^o might depend on the overall level of amorphous orientation and/or the *trans/gauche* ratio of the polymer sample. It can be argued, similarly, that Δ_c^o would be influenced by crystal imperfections, such as lattice distortions and vacancies. As a conceptual aid to this notion of intrinsic birefringence, one could imagine inserting at random a number of fully oriented chains into the amorphous and crystalline regions of the polymer sample, and then (somehow) measuring the average birefringence of these chains in the two environments. Since neither of these environments is necessarily homogeneous or fully oriented, their particular state of disorder would influence the birefringent properties of the oriented chains.

Until the recent analysis of Gupta and Ramesh[39], there was little direct evidence to support the notion that Δ_c^o and Δ_a^o are dependent on the structural state of the polymer. The wide variations in the experimentally determined values of intrinsic birefringence reported for PET have usually been attributed to inadequacies in the experimental methods used[40,41], and there are a number of sound arguments for this interpretation.

Since equation (16) can be recast as:

$$\frac{\Delta}{\chi\langle P_2(\cos\Theta)\rangle_c} = \Delta_c^o + \left[\frac{1-\chi}{\chi}\right]\frac{\langle P_2(\cos\Theta)\rangle_a}{\langle P_2(\cos\Theta)\rangle_c}\Delta_a^o \tag{18}$$

a common procedure for determining the intrinsic birefringences involves plotting $\Delta/\chi\langle P_2(\cos\Theta)\rangle_c$ against $[(1-\chi)/\chi][\langle P_2(\cos\Theta)\rangle_a/\langle P_2(\cos\Theta)\rangle_c]$, to yield Δ_c^o as intercept and Δ_a^o as slope. The problems arise in the determination of amorphous orientation, $\langle P_2(\cos\Theta)\rangle_a$, for this plot. The most frequently used technique has been 'sonic modulus', involving sonic velocity measurements along a specimen held under a very small load[42,43]. The amorphous orientation is given by[43]:

$$\langle P_2(\cos\Theta)\rangle_{a/\text{sonic}} = \left[\frac{3}{2(E_u - E)} - \frac{\chi\langle P_2(\cos\Theta)\rangle_c}{E_{t,c}^o}\right]\frac{E_{t,a}^o}{(1-\chi)} \tag{19}$$

where E is the sonic modulus of the oriented specimen, E_u is the sonic modulus of an unoriented reference specimen and $E_{t,c}^o$ and $E_{t,a}^o$ are the intrinsic transverse moduli of the crystalline and amorphous regions, respectively. Various aspects of this technique cast doubt on its reliability. It assumes that for amorphous chains, the linear relationship between sonic modulus and birefringence at low orientations[26,42] extends to higher orientations where the relationship is likely to be more complex[44,45], and where its experimental determination is precluded by the presence of crystallinity. Also uncertain is the assumption that $E_{t,c}^o$ and $E_{t,a}^o$ are material constants, unaffected by processing history. Finally there may be validity in the suggestion that the sound wave propagates preferentially along the taut tie molecules, resulting in values of amorphous orientation which are higher than the true average.

Amorphous orientation data from infra-red (Fourier transform infra-red, *FT*i.r.) analysis were recently used to determine the intrinsic birefringences of PET[39]. The amorphous orientation values were calculated from[46]:

$$\langle P_2(\cos\Theta)\rangle_{a/FT\,\text{i.r.}} = \frac{[m_{trans}\langle P_2(\cos\Theta)\rangle_{trans}] - [\chi\langle P_2(\cos\Theta)\rangle_c]}{(1-\chi)} \tag{20}$$

where m_{trans} is the fraction of *trans* material, obtained from the *trans/gauche* ratio, and $\langle P_2(\cos\Theta)\rangle_{trans}$ is the orientation average of all the *trans* material (crystalline and non-crystalline). This formulation assumes that the orientation of chain segments in the *gauche* conformation is always isotropic.

A disadvantage of both the sonic modulus and *FT*i.r. techniques is that they require measurement of numerous parameters, including crystallite orientation and the degree of crystallinity, which can lead to appreciable scatter in the orientation value calculated. In the various studies of the intrinsic birefringence of PET, X-ray diffraction has been the only truly direct method used to obtain the amorphous orientation[47]. Since one cannot reliably measure amorphous orientation from WAXS when crystalline reflections are present, this method cannot be used to determine Δ_c^o, but is suitable for determining Δ_a^o. However, since the amorphous orientation of the specimens must be low to avoid crystallization, in order to obtain Δ_a^o it is necessary to linearly extrapolate a plot of $\langle P_2(\cos\Theta)\rangle_a$ *versus* Δ to $\langle P_2(\cos\Theta)\rangle_a = 1$. Because there is some evidence that the relationship between $\langle P_2(\cos\Theta)\rangle_a$ and Δ is non-linear at high orientations[48], this procedure is uncertain.

Clearly, the methods used so far to obtain amorphous orientation for intrinsic birefringence determinations involve various simplifications which may be unreason-

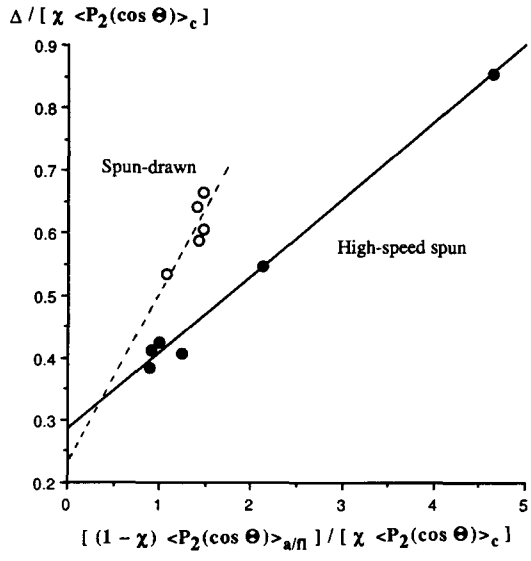

Figure 13 Plot for determination of 'intrinsic' birefringence values of the amorphous and crystalline phases of PET (Δ_a^o and Δ_c^o)

able, but it is difficult to assess the extent of their influence on the calculated orientation value. Since the polarized intrinsic fluorescence method appears to permit *direct* measurement of average amorphous orientation, and seems not to involve significant simplifications, it provides a new opportunity to shed light on the nature of intrinsic birefringence in PET.

Using amorphous orientation data from intrinsic fluorescence and plotting in accordance with equation (18) results in a good linear fit for the high-speed spun fibres (*Figure 13*), and yields $\Delta_a^o = 0.12$ and $\Delta_c^o = 0.28$. For the spun-drawn fibres there are too few data points to be sure that they all lie on a single line, but clearly the intrinsic birefringences must be significantly different from those of the high-speed spun fibres. Values of $\Delta_a^o = 0.27$ and $\Delta_c^o = 0.24$ would adequately fit all the spun-drawn data. According to the model of Nobbs *et al.*[49], significant densification of the amorphous phase would occur when amorphous orientation exceeds ~0.4. It is noteworthy that correcting for this effect in the determination of crystallinity would somewhat enlarge the differences between the high-speed spun and spun-drawn data in *Figure 13*.

Our Δ_a^o value of 0.12, obtained from high-speed spun fibres, is much lower than that usually reported for PET, especially Dumbleton's value of 0.275 obtained from a series of spun-drawn fibres[26]. It is consistent, however, with results from high-speed spun fibres reported by Garg[41] and by Perez and Lecluse[50]. Convinced that the intrinsic birefringences of PET should be independent of specimen preparation, Garg rejected his low value of Δ_a^o, as well as the values of Dumbleton and of Perez and Lecluse, arguing that the sonic modulus technique depends on dubious assumptions. He therefore adopted an alternative method for determining Δ_a^o, based on the stress–birefringence relationships predicted by Gaussian rubber elasticity theory, and obtained a value of 0.19. However, the universal applicability of Gaussian assumptions to the deformation of PET is in doubt[51–53].

Our result of $\Delta_c^o = 0.28$, for the high-speed spun fibres, is higher than most of the published values for PET, but is close to values reported by Gupta and Kumar[54]. Moreover, Gupta and Kumar[55] have recently produced a semicrystalline PET fibre with an *overall* birefringence of 0.26, indicating that Δ_c^o must significantly exceed 0.26, at least for this fibre.

Although preliminary, our fluorescence study indicates that the variations in Δ_c^o and Δ_a^o reported in the literature may arise predominantly from a real dependence on microstructure, and that the influence of experimental artifact may be relatively small. In our current experiments, we are attempting to determine whether Δ_c^o and Δ_a^o have systematic relationships with specific structural features. One would expect, for example, that improving crystal perfection by heat treatment would result in higher Δ_c^o. Our present data fall into two orientation ranges, varying between 0.22 and 0.32 for the high-speed spun fibres and between 0.45 and 0.55 for the spun-drawn fibres. To investigate the influence of amorphous orientation on Δ_a^o, specimens with intermediate orientations are being prepared, by drawing the high-speed spun fibres and by shrinking the spun-drawn fibres.

CONCLUDING REMARKS

Further exploration and development of the chain-intrinsic fluorescence technique have confirmed its suitability as a means to measure molecular orientation in the non-crystalline regions of PET. The results from fibre and film are in good qualitative agreement with results from other methods and bear out, for example, the expected role of orientation on the induction and development of crystallinity during drawing. Moreover, we would expect the absolute orientation values obtained from intrinsic fluorescence to be of superior accuracy: the method involves far fewer assumptions and measurements than other techniques, and our improved experimental set-up minimizes measurement errors. Intrinsic fluorescence is particularly suited, therefore, to detailed fundamental studies, such as the nature of the structural dependence of 'intrinsic' birefringence and the testing and development of deformation models[53]. Further experience with this technique will permit continuing assessment of its capabilities.

ACKNOWLEDGEMENTS

This study is one aspect of work on two TRI projects, 'Structure and Properties of Poly(ethylene Terephthalate) Film' and 'Dye Transport Phenomena and Fiber Structure', each supported by a group of Corporate TRI Participants. The authors are grateful to Dennis W. Briant, Sigrid B. Ruetsch and Lei Zhang of the TRI staff for assistance with the experimental work, and to Dr H.-D. Weigmann for his encouragement.

REFERENCES

1 Nishijima, Y., Onogi, Y. and Asai, T. *J. Polym. Sci. C* 1966, **15**, 237
2 Nishijima, Y., Fujimoto, T. and Onogi, Y. *Rep. Prog. Polym. Phys. Jpn* 1966, **9**, 457
3 Nishijima, Y., Onogi, Y. and Asai, T. *Int. Symp. Macromol. Chem.* 1966, **7**, 161
4 Nishijima, Y., Onogi, Y. and Asai, T. *Rep. Prog. Polym. Phys. Jpn* 1967, **10**, 465
5 Nishijima, Y., Onogi, Y., Asai, T. and Yamazaki, R. *Rep. Prog. Polym. Phys. Jpn* 1967, **10**, 465
6 Nishijima, Y. and Onogi, Y. *Rep. Prog. Polym. Phys. Jpn* 1968, **11**, 395
7 Nishijima, Y., Onogi, Y., Asai, T. and Yamazaki, R. *Rep. Prog. Polym. Phys. Jpn* 1968, **11**, 399, 403

8 Nishijima, Y. and Asai, T. *Rep. Prog. Polym. Phys. Jpn* 1968, **11**, 419, 423
9 Desper, C. R. and Kimura, I. *J. Appl. Phys.* 1967, **38**, 4225
10 Nobbs, J. H., Bower, D. I., Ward, I. M. and Patterson, D. *Polymer* 1974, **15**, 287
11 Stein, R. S. *J. Polym. Sci. A2* 1968, **6**, 1975
12 White, J. L. and Spruiell, J. E. *Polym. Eng. Sci.* 1981, **21**, 859
13 Nobbs, J. H., Bower, D. I. and Ward, I. M. *J. Polym. Sci., Polym. Phys. Edn* 1979, **17**, 259
14 Allen, N. S. and McKellar, J. F. *Makromol. Chem.* 1978, **179**, 523
15 Hennecke, M. and Fuhrmann, J. *Makromol. Chem., Macromol. Symp.* 1986, **5**, 181
16 Hennecke, M., Kud, A., Kurz, K. and Fuhrmann, J. *Colloid Polym. Sci.* 1987, **265**, 674
17 Hemker, D. J., Frank, C. W. and Thomas, J. W. *Polymer* 1988, **29**, 437
18 Sonnenschein, M. F. and Roland, C. M. *Polymer* 1990, **31**, 2023
19 Hennecke, M. Personal communication, 1991
20 Hennecke, M. and Fuhrmann, J. *Colloid Polym. Sci.* 1980, **258**, 219
21 Pinaud, F., Jarry, J. P., Sergot, Ph. and Monnerie, L. *Polymer* 1982, **23**, 1575
22 Fuhrmann, J. and Hennecke, M. *Colloid Polym. Sci.* 1976, **254**, 6
23 Salem, D. R. *Polymer* 1992, **33**, 3182
24 Salem, D. R. *Polymer* 1992, **33**, 3189
25 Stein, R. S. and Norris, F. H. *J. Polym. Sci.* 1956, **21**, 381
26 Dumbleton, J. H. *J. Polym. Sci. A2* 1968, **6**, 795
27 Heuvel, H. M., Huisman, H. and Lind, K. C. J. B. *J. Polym. Sci., Polym. Phys. Edn* 1976, **14**, 921
28 Heuvel, H. M. and Huisman, R. *J. Appl. Polym. Sci.* 1978, **22**, 2229
29 Huisman, R. and Heuvel, H. M. *J. Appl. Polym. Sci.* 1978, **22**, 943
30 Salem, D. R. unpublished data
31 Northolt, M. G. and Stutt, H. A. *J. Polym. Sci., Polym. Phys. Edn* 1978, **16**, 939
32 Salem, D. R. *J. Polym. Sci. B, Polym. Phys.* 1987, **25**, 2561
33 Le Bourvellec, G., Monnerie, L. and Jarry, J. P. *Polymer* 1986, **27**, 856
34 Buckley, C. P. and Salem, D. R. *Polymer* 1987, **28**, 69
35 Padhye, M. R. and Tamhane, P. S. *Angew. Makromol. Chem.* 1978, **69**, 33
36 Ziabicki, A. and Jarecki, K. in 'High Speed Fiber Spinning' (Eds A. Ziabicki and H. Kawai), John Wiley and Sons, New York, 1985, Ch. 9, p. 225
37 Salem, D. R. and Weigmann, H.-D. *J. Polym. Sci. B, Polym. Phys.* 1991, **29**, 765
38 Stein, R. S. *J. Polym. Sci. C* 1966, **15**, 185
39 Gupta, V. B. and Ramesh, C. *Polym. Commun.* 1987, **28**, 43
40 Vassilatos, G., Knox, B. H. and Frankfort, H. R. E. in 'High Speed Fiber Spinning' (Eds A. Ziabicki and H. Kawai), John Wiley and Sons, New York, 1985, Ch. 14, p. 418
41 Garg, S. *J. Appl. Polym. Sci.* 1982, **27**, 2857
42 Moseley, W. W. *J. Appl. Polym. Sci.* 1960, **3**, 266
43 Samuels, R. J. *J. Polym. Sci. A* 1965, **3**, 1741
44 Ward, I. M. 'Mechanical Properties of Solid Polymers', John Wiley and Sons, New York, 1971
45 Ward, I. M. *Textile Res. J.* 1964, **34**, 806
46 Padibjo, S. R. and Ward, I. M. *Polymer* 1983, **24**, 1103
47 Biangardi, H. J. *J. Polym. Sci., Polym. Phys. Edn* 1980, **18**, 903
48 Zachmann, H. G. *Polym. Eng. Sci.* 1979, **19**, 966
49 Nobbs, J. H., Bower, D. I. and Ward, I. M. *Polymer* 1976, **17**, 25
50 Perez, G. and Lecluse, C. *18 Int. Chemiefasertagung Dornbirn* 1979, **20**, no. 22
51 Brown, D. J. and Windle, A. H. *J. Mater. Sci.* 1984, **19**, 1997
52 Brown, D. J. *Polym. Commun.* 1985, **26**, 42
53 Clauss, B. and Salem, D. R. in preparation
54 Gupta, V. B. and Kumar, S. *J. Polym. Sci., Polym. Phys. Edn* 1979, **17**, 1307
55 Gupta, V. B. and Kumar, S. *Polym. Commun.* 1989, **30**, 341